Science of the Total Environment 616–617 (2018) 208–222

Contents lists available at ScienceDirect

Science of the Total Environment

journal homepage: www.elsevier.com/locate/scitotenv

Modeling future water footprint of barley production in Alberta, Canada: Implications for water use and yields to 2064

Mohammad Badrul Masud [a,*], Tim McAllister [b], Marcos R.C. Cordeiro [b], Monireh Faramarzi [a]

[a] Department of Earth and Atmospheric Sciences, Faculty of Science, University of Alberta, 1-26, Earth Sciences Building, Edmonton, T6G 2E3, Alberta, Canada
[b] Science and Technology Branch, Agriculture and Agri-Food Canada, Lethbridge Research and Development Centre, 5403–1 Avenue South, P.O. Box 3000, Lethbridge, T1J 4B1, Alberta, Canada

HIGHLIGHTS

- A framework is developed to model barley yield, water use and water footprint.
- Yield and water footprint of barley is assessed under climate change.
- Rainfed yield is projected to increase and irrigated yield is expected to remain unchanged.
- Water footprint is projected to decrease in future.
- Water footprint is adjusted based on water-stress conditions.

GRAPHICAL ABSTRACT

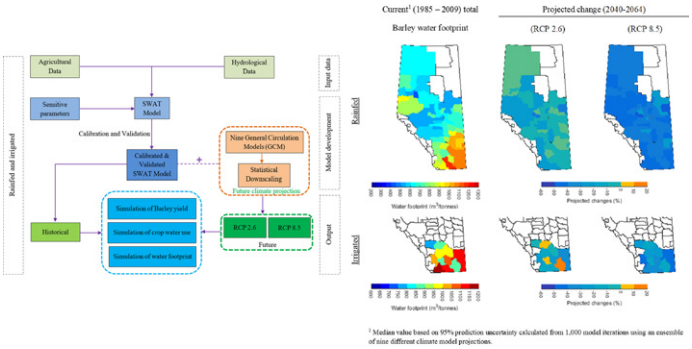

ARTICLE INFO

Article history:
Received 22 August 2017
Received in revised form 31 October 2017
Accepted 1 November 2017
Available online 16 November 2017

Editor: D. Barcelo

Keywords:
Crop modeling
Water stress
Blue and green water footprint
Uncertainty prediction
Climate change

ABSTRACT

Despite the perception of being one of the most agriculturally productive regions globally, crop production in Alberta, a western province of Canada, is strongly dependent on highly variable climate and water resources. We developed agro-hydrological models to assess the water footprint (WF) of barley by simulating future crop yield (Y) and consumptive water use (CWU) within the agricultural region of Alberta. The Soil and Water Assessment Tool (SWAT) was used to develop rainfed and irrigated barley Y simulation models adapted to sixty-seven and eleven counties, respectively through extensive calibration, validation, sensitivity, and uncertainty analysis. Eighteen downscaled climate projections from nine General Circulation Models (GCMs) under the Representative Concentration Pathways 2.6 and 8.5 for the 2040–2064 period were incorporated into the calibrated SWAT model. Based on the ensemble of GCMs, rainfed barley yield is projected to increase while irrigated barley is projected to remain unchanged in Alberta. Results revealed a considerable decrease (maximum 60%) in WF to 2064 relative to the simulated baseline 1985–2009 WF. Less water will also be required to produce barley in northern Alberta (rainfed barley) than southern Alberta (irrigated barley) due to reduced water consumption. The modeled WF data adjusted for water stress conditions and found a remarkable change (increase/decrease) in the irrigated counties. Overall, the research framework and the locally adapted regional model results will facilitate the development of future water policies in support of better climate adaptation strategies by providing improved WF projections.

1. Introduction

Canada is home to ~12 million head of cattle with the majority of beef production occurring in Alberta (Farm Credit Canada, 2012). Alberta is globally recognized for its large oil and agricultural exports

* Corresponding author.
E-mail address: masud@ualberta.ca (M.B. Masud).

https://doi.org/10.1016/j.scitotenv.2017.11.004
0048-9697/

including beef and live cattle to over 50 countries around the world (Alberta Cattle Feeders' Association, 2017). Beef production in this province depends largely on annual feed crops such as wheat, canola, and barley, with barley being the principal feed. Given that global beef production is expected to increase 74% by 2050 (FAO, 2017), there will be an increased need to produce barley to sustain Alberta beef exports. Water use intensity of beef production in Canada indicates that feed and pasture production are responsible for the majority of water consumption (Legesse et al., 2017). However, unreliable precipitation patterns, potentially adverse impacts due to climate change, and increasing conflicts among different water users represent serious challenges to the availability of this critical resource for Alberta's beef industry (Islam and Gan, 2014; de Souza et al., 2017). Thus, an assessment of barley production in the future in light of the uncertainties in water availability arising from climate change is needed in order to prepare the beef industry for potential issues that can compromise its sustainability in Alberta and its contribution to global food security.

A usable metric for assessing current and future crop water use is water footprint (WF) accounting, which offers a quantifiable indicator to measure the volume of consumptive water use (CWU) per unit crop yield (Y). The WF of crops can be quantified as being composed of blue, green, and grey forms (Hoekstra et al., 2011). The blue WF of crops is based on freshwater consumption (e.g., lakes, river, and aquifers), while green WF is based on effective precipitation that is consumed in the form of soil moisture. The grey WF is quantified based on the amount of freshwater required to assimilate pollutants to meet specific water quality standards. Application of the water footprint concept has been particularly challenging at large-scale studies (Marano and Filippi, 2015; Ma and Ma, 2017; Shrestha et al., 2017a), due to uncertainties in representing soil-plant-water-atmosphere relationships at the regional scale, where changes in water consumption and crop yields are influenced by both natural and anthropogenic factors. In this context, future projections of crop production in relation to climate change involve interactive and dynamic soil-plant-atmosphere processes that are assessed with integrated system models (Ahuja et al., 2007).

One example of such models is the Soil and Water Assessment Tool (SWAT), a process-based, time-continuous, bio-physical model (Arnold et al., 1998) that simulates hydrology and soil-water dynamics at a daily time step (Vigiak et al., 2015). It is widely used to simulate the impacts of climate, water, and agricultural management practices on hydrology, vegetation growth, and related bio-physical processes in small and large basins (Tuo et al., 2016). SWAT has been used in a number of large and regional scale studies (Abbaspour et al., 2015; Vigiak et al., 2015; Palazzoli et al., 2015; Liu et al., 2017; Faramarzi et al., 2017; Shrestha et al., 2017a).

It is hypothesized that barley production and its water use in Alberta can satisfactorily be projected by considering the key influential factors and adapting to the regional/local conditions using the SWAT model. The main objective of this study is to assess the WF of barley as the principal feed crop used in beef cattle production. The specific objectives are: 1) to set up a high-resolution crop model of Alberta for rainfed and irrigated barley by utilizing available local agro-hydrologic data and information; 2) to adjust physical parameters of the rainfed and irrigated models to local conditions by calibration and validation of annual crop yields; 3) to project future climate change impacts on Y, CWU, and blue and green WF of rainfed and irrigated barley; and to address the most influential bio-physical factors affecting the likely changes; and 4) to adjust the results to local water stress conditions.

2. Methods and data

2.1. Study area

Alberta is a semi-arid western province in Canada with an area spanning 661,000 km^2 (Fig. 1a,b). It has a highly variable climate with mean annual precipitation ranging from ≈280 mm in the south to ≈1000 mm at the higher elevations of the Rocky Mountains (Masud et al., 2015). Mean winter temperatures usually range from −25.1 to −9.6 °C while mean summer temperatures vary between 8.7 and 18.5 °C with the mean annual temperature ranging from 3.6 to 4.4 °C (Jiang et al., 2017). The province has 17 river basins (Fig.1a). Most of the southern river basins are snowmelt dominated in their upstream highland areas, and glacier melt plays a major role in supplying downstream water needs in late summer.

Alberta is the home of 65% irrigation in Canada (Alberta WaterPortal, 2017). With 6% of Alberta's total water availability (Faramarzi et al., 2017), the southern river basins provide nearly 57% of the irrigation water in 13 irrigation districts (Fig. 1c). The government of Alberta is seeking means of improving water use efficiency, and reducing the water footprint to meet water supply-demand constraints during periods of high water shortages (Faramarzi et al., 2017). Irrigation districts are spread in 11 out of 67 counties (Fig. 1c) in the southern part of the province, where there is often not sufficient precipitation and soil moisture to naturally meet crop requirements. In the central and northern areas of the province crop production relies on precipitation. Barley is one of the most commonly grown crops in the province, and its production and Y is dependent on the availability of water resources and influenced by other climate and phenological factors. For instance, rainfed barley had an average annual yield of 2.5 t/ha, dropped to its lowest level (1.5 t/ha) in 2002, due to drought, generating the lowest yield during the 25-year period (1983–2007). While irrigated yield sustained around 4.5 t/ha with sufficient irrigation to compensate climate variations (Fig. 1d,e).

2.2. SWAT overview

The SWAT model divides each river basin into sub-basins based on topography and subsequently into Hydrologic Response Unit (HRU) according to the soil, land use, and slope characteristics. The plant growth component of SWAT, which is a simplified version of the Erosion Productivity Impact Calculator (EPIC; ref. Williams, 1995), is capable of simulating a wide range of crops, grassland, and pasture. In the SWAT model, crop biomass development (above- and- under ground) is simulated on a daily time-step based on light interception and conversion of CO_2 to biomass. Actual crop yield is then calculated as a product of actual above ground biomass and the actual harvest index. Actual harvest index is calculated, on a daily basis, as a fraction of above ground plant dry biomass removed as dry economic yield. A plant is assumed to start growing once the temperature exceeds its base temperature (T_b). The portion of the mean daily temperature exceeding T_b will contribute to growth over the growing period. If the temperature falls below T_b then the plant is assumed to enter dormancy. The actual crop water uptake is simulated in a daily time step. It is based on soil water dynamics in different soil layers and crop potential evapotranspiration (PET). There are three different methods (i.e. Penman-Monteith, Priestley-Taylor, and Hargreaves) available in the model to calculate PET, with the Penman-Monteith being the most comprehensive as it considers various climatic factors (Allen et al., 1989). The Penman-Monteith approach was considered in this study as the base to simulate CWU.

In this study, four and five management practices were selected for rainfed and irrigated condition, respectively. The practices were ploughing, fertilizer application, irrigation, planting operation and harvest and kill operations. Two options are available for application of irrigation water and timing of fertilizer application: user specified and automatic. In the automatic option, an irrigation event is triggered by water stress threshold and fertilizer is applied based on nutrients stress factor. The total amount of fertilizer applied during the growing season is specified by the user. More details are given by Neitsch et al. (2011).

2.3. Input data, model development and parameterization

In this study, ArcSWAT 2012 (Rev. 632) was used to set up the model. A hydrology model of the province, developed and calibrated in an

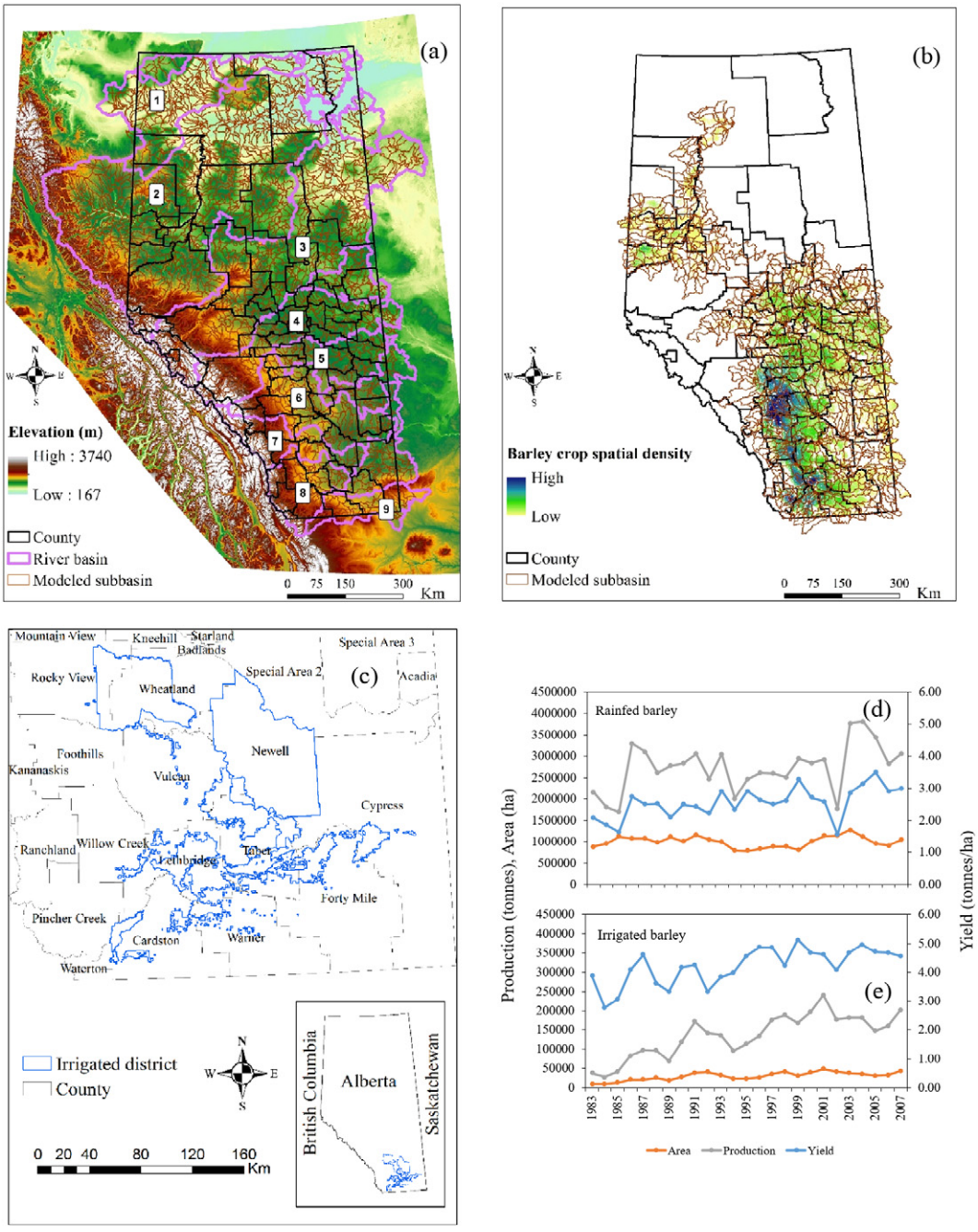

Fig. 1. (a) Map of the study area with 2255 sub-basins, (b) Alberta agricultural region containing 67 counties and 970 sub-basins, and (c) Alberta irrigation districts containing 231 sub-basins across 11 counties. The barley crop spatial density is also shown in (b,c). Historical yield, production, and area for (d) rainfed and (e) irrigated barley as reported by AFSC are shown. List of 9 major river basins out of 17 in (a): 1-Hay River Basin (RB); 2-Peace RB; 3-Athabasca RB; 4-North Saskatchewan RB; 5-Battle RB; 6-Red Deer RB; 7-Bow RB; 8-Oldman RB; 9-Milk RB.

earlier study by Faramarzi et al. (2017), was used as the base model to develop the crop growth model. In the hydrology model a threshold of 200 km^2 was used to delineate the study area into a total of 2255 sub-basins based on a 10 m Digital Elevation Map (DEM). Further, the sub-basins were characterized based on soil, land use, and slope maps and associated physical parameters available from local sources and further processed to meet the model requirements (Faramarzi et al., 2017). Daily climate data (i.e. precipitation, temperature, solar radiation, humidity, and wind speed) were based on an earlier study by Faramarzi et al. (2015), where a suit of four climate time series from meteorological, gridded products, and satellite data were examined at a provincial coverage to reproduce historical flow records by using the SWAT model. A "combination" approach, where various climate data were combined from different sources, was found to be best in generating their corresponding streamflow data. Other hydrological data (i.e. potholes, daily operation of large reservoirs and large dams and glacial maps) were also incorporated in the model to better represent hydrological processes at sub-basin levels. To simulate barley growth, we developed and calibrated two separate models for rainfed and irrigated barley by using a previously calibrated hydrology model as the base in both models. Setting up a crop growth model based on a calibrated hydrologic model has been recommended to improve soil-water dynamics in crop growth simulations (Faramarzi et al., 2010; Azimi et al., 2013; Vaghefi et al., 2014). Yearly Y statistics for irrigated and rainfed barley

in 11 and 67 counties were obtained from Alberta Financial Service Corporation (AFSC), respectively for the 1980–2009 period for the purpose of model calibration and validation.

Agricultural management data, (i.e., date of planting and harvesting, volume, and rate of fertilizer and irrigation application) were needed to develop the SWAT crop model. The crop-specific fertilizer application rate (N:P:K ratio), the maximum amount of annual fertilizer application (kg/ha per year), and the potential heat units required for barley were obtained from a Government of Alberta (Alberta Agriculture and Rural Development, 2004). Heat unit requirements were further optimized through our calibration procedure to represent different varieties of barley that differ in growing degree days across counties. Auto fertilizer and auto irrigation options of the SWAT model were used based on the assumption that farmers were using good management practices. Planting and harvesting dates were obtained from literature and communication with local experts. Since the cropping calendar did not fully encompass the scale of this study, the suggested dates were further optimized through our calibration scheme (see later sections for calibration).

2.4. Sensitivity, calibration, validation and uncertainty analysis

For sensitivity, calibration, validation and uncertainty analysis, the Sequential Uncertainty Fitting (SUFI-2) program of the SWAT-CUP software was used. The SWAT-CUP is linked to SWAT model and provides a sound basis for multi-site calibration, validation, uncertainty analysis, as well as large-scale parameterization through a parallelization scheme. The SUFI-2 was used in this study to calibrate the model from 1995 to 2009 and to validate it for the 1983–1994 period. A three-year window was considered as a warm-up period for both calibration and validation to mitigate the effect of initial unknown conditions in the model. The inverse chronology was used for calibration and validation since better data were available in the later period. SUFI-2 is widely used mainly due to the fewer number of model runs needed to reach acceptable calibration results as compared to other calibration techniques (e.g., Generalized Likelihood Uncertainty Estimation (GLUE) (Beven and Binley, 1992); Parameter Solution (ParaSol) (van Griensven and Meixner, 2006); and a Monte Carlo Markov Chain (MCMC) (Vrugt et al., 2003) algorithm).

Based on an extensive literature review and author's judgment, a set of 29 and 32 physical and phenological parameters were selected for each county for rainfed and irrigated crop growth simulation, respectively (Table 1). A global sensitivity analysis (GSA) was applied through the SWAT-CUP tool to screen the most sensitive parameters. The parameters were then sampled using a Latin Hypercube Sampling (LHS) approach (Mckay et al., 1979) and performed 1000 model runs. The mean square error (MSE) was used as an objective function to compare simulated versus observed Y on a yearly basis for each county.

$$MSE = \frac{1}{n}\sum_{i=1}^{n}(O_i - S_i)^2 \quad (1)$$

where n is the number of observed yields in each county, O is the observed yield, and S is the simulated yield for each individual county. The GSA was used because it varies all parameters simultaneously and provides robust sensitivity measures in the presence of nonlinear responses and interactions among model parameters (Liu et al., 2014; Wainwright et al., 2014; Prowse et al., 2016). The GSA was measured by the value of t-test and associated probability level of the regression coefficient of each parameter against the objective function. A parameter with higher absolute t-value indicates higher sensitivity and vice-versa.

The calibration was conducted through an iterative procedure, where the initial ranges of sensitive parameters (Table 1) were chosen in the first iteration. The initial ranges are large in quantity but physically meaningful to ensure simulated crop yield close to previously reported yield data (Vu et al., 2012; Grusson et al., 2015; Tuo et al., 2016). After each iteration of 1000 simulations, the range of parameters were narrowed based on suggested new ranges by the SUFI-2, their physical limitations, and local agro-hydrological knowledge. In SUFI-2, the new parameter ranges were centered on the most recent and the best simulation based on the best objective function value for the subsequent iterations. A maximum five iterations were suggested by Abbaspour (2015), with four being applied in this study. This iterative calibration was conducted for each county separately to account for the large spatial heterogeneity of the geophysical and agricultural conditions. More details about the calibration protocol are available in Abbaspour et al. (2015). In SUFI-2, the 95% prediction uncertainty (95PPU) of the output variables were considered to evaluate the model performance. The 95PPU is calculated at the 2.5% and 97.5% levels of the cumulative distribution functions of an output variable that is generated through the propagation of the parameter uncertainties using LHS. Parameter uncertainty here accounts for various sources of uncertainties including input uncertainty, structural uncertainty, as well as parameter uncertainty (Faramarzi et al., 2017). The p-factor and r-factor are used to quantify calibration performance. The p-factor is the percentage of observed data bracketed by the 95PPU, and the r-factor is the thickness of the 95PPU, which is calculated as the ratio of the average width of the 95PPU to the standard deviation of the measured variable. Ideally, a p-factor value of 1 and a r-factor value of zero is expected, however in large-scale studies due to inherent uncertainties in input data, physical parameters, and model conceptualization the p-factor of above 0.5 and r-factor of around 1–2 is considered as satisfactory in hydrologic studies (Abbaspour et al., 2007, 2015; Shrestha et al., 2017b). However, an r-factor of 3–5 would be reasonable for yield calibrations since standard deviation of the yield data are smaller than that of the hydrologic flow data. The mean square error (MSE) was used in this study as a goodness-of-fit indicator for the best simulation of barley yields. In this study yields were simulated at sub-basin scale and then aggregated to county scale for comparison purposes. The model runs were parallelized in several 40-core computers that utilized parallel processing option of the SWAT-CUP software.

2.5. Climate projections from GCMs

General Circulation Models (GCMs) are physical based tools that provide a reasonable basis for estimating future climate. However, the output from GCMs cannot be applied directly in many regional or local agricultural, environmental, and water resource studies due to poor representation and simulation of local-scale processes and coarse spatial resolution (Masud et al., 2016). Therefore, downscaling of GCM outputs is necessary before application in the impact studies, e.g., calibrated SWAT model. The climate projection of nine GCMs for the 2040–2064 period was obtained from the Pacific Climate Impacts Consortium (PCIC; Cannon, 2015) at a resolution of 300 arc *sec* (~10 km) and was used for the study (Table 2). The GCM outputs (i.e., daily precipitation, minimum and maximum temperature) under two extreme scenarios of the Representative Concentration Pathways, i.e., RCP 2.6 and 8.5, were used to project mid-21st century (2040–2064) climate scenarios for the study area. RCP defines a specific emissions trajectory and subsequent radiative forcing in the earth-atmosphere system. The RCP 2.6 represents a very low greenhouse gas (GHG) concentration (CO_2 equivalent 490 ppm) and a peak in radiative forcing of approximately 3 Wm^{-2} before 2100, declining to 2.6 Wm^{-2} by 2100. The RCP 8.5 is characterized by high GHG concentration (CO_2 equivalent 1370 ppm) and indicates a rising pathway leading to 8.5 Wm^{-2} by 2100 (IPCC, 2014). In this study, we set the concentration of CO_2 as 350, 450, and 750 ppm for the historical, RCP 2.6, and RCP 8.5, respectively.

Although PCIC used the bias-correction spatial disaggregation (BCSD) approach following the methodology of Maurer and Hidalgo (2008) to downscale the data for all of Canada, the change factor approach (Chen et al., 2011; Basheer et al., 2016; Tan et al., 2017) under statistical downscaling, which is an approach to establish an empirical relationship between GCM and historical data in order to generate a downscale GCM output, was used in this study, based on the local climate conditions of

Table 1
Initial parameter ranges for sensitivity analysis and calibration.

No	Parameter	Definition	Initial range[a]
1	v__DAY{[],1}.mgt	Day operation takes place	1–15
2	v__HEAT_UNITS{[],1}.mgt	Total heat units for plant to reach maturity	1800–2300
3	v__AUTO_NSTRS{[],11}.mgt	Nitrogen (N) stress factor of plant that triggers fertilization	0.85–0.95
4	v__AUTO_NAPP{[],11}.mgt	Maximum amount of mineral N allowed in any one application (kg N/ha)	30–40
5	v__AUTO_NYR{[],11}.mgt	Maximum amount of mineral N allowed to be applied in any one year (kg N/ha)	57–77
6	v__AUTO_EFF{[],11}.mgt	Application efficiency	1–1.2
7	v__AFRT_SURFACE{[],11}.mgt	Fraction of fertilizer applied to top 10 mm of soil	0.2–0.5
8	v__AUTO_WSTRS{[],10}.mgt	Water stress threshold that triggers irrigation	0.85–0.95[b]
9	v__IRR_EFF{[],10}.mgt	Irrigation efficiency	70-85[b]
10	v__IRR_MX{[],10}.mgt	Amount of irrigation water applied each time auto irrigation is triggered (mm)	20-50[b]
11	r__CN2.mgt	SCS runoff curve number for moisture condition II	−0.4–0.4
12	v__ESCO.hru	Soil evaporation factor	0.01–1
13	v__EPCO.hru	Plant uptake compensation factor	0.01–1
14	v__OV_N.hru_	Manning's n value for overland flow	0.01–0.8
15	v__LAT_TTIME.hru	Lateral flow travel time (days)	0–180
16	v__LAT_SED.hru	Sediment concentration in lateral and groundwater flow (mg/L)	0–5000
17	r__CANMX.hru	Maximum canopy storage (mm H_2O)	0–0.3
18	r__HRU_SLP.hru	Average slope steepness (m/m)	−0.4–0.4
19	r__SOL_BD(1).sol	Soil bulk density in layer 1 of soil profile (g/cm3)	−0.4–0.4
20	r__SOL_CBN(1).sol	Organic carbon content in layer 1 of soil profile (% soil weight)	−0.4 - -0.1
21	r__SOL_ALB(1).sol	Moist soil albedo in layer 1 of soil profile	−0.4–0.4
22	r__ANION_EXCL.sol	Fraction of porosity from which anions are excluded	0–0.3
23	r__SOL_K(1).sol	Saturated hydraulic conductivity in layer 1 of soil profile (mm/h)	−0.4–0.4
24	r__SOL_CRK.sol	Potential or maximum crack volume of the soil profile	−0.4–0.4
25	r__USLE_K(1).sol	USLE equation soil erodibility (K) factor in layer 1 of soil profile	−0.4–0.4
26	r__SOL_AWC().sol	Available water capacity of the soil layer (mm H_2O/mm soil)	−0.5–0.4
27	v__SHALLST.gw	Initial depth of water in the shallow aquifer (mm H_2O)	0–1000
28	v__ALPHA_BF.gw	Baseflow alpha factor (1/days)	0–1
29	v__SHALLST_N.gw	Initial concentration of nitrate in shallow aquifer (mg N/L or ppm)	0–10
30	v__GW_SPYLD.gw	Specific yield of the shallow aquifer (m3/m3)	0–0.4
31	v__GWSOLP.gw	Concentration of soluble phosphorus in groundwater (mg N/L or ppm)	0–1000
32	v__HLIFE_NGW.gw	Half-life of nitrate in the shallow aquifer (days)	0–365

[a] Minimum and maximum values of the parameter range over 67 counties. v and r indicate absolute and relative value, respectively.
[b] These three parameters were not considered for rainfed barley.

Alberta. Here, the historical climate data were used from Faramarzi et al. (2015), where an extensive qualification was conducted on different sets of historical station-based and gridded data. Overall, an ensemble of eighteen different climate model projections were downscaled and fed into the calibrated SWAT model under various GCMs and RCP scenarios. For each GCM and RCP, a total of 1000 SWAT simulations were performed on daily basis using the calibrated parameter ranges. Then the L95PPU and U95PPU as well as M95PPU (median of 1000 simulations) were obtained for aggregated monthly and yearly outputs at sub-basin and county levels. The multi-model results were then averaged to discuss the projected changes on Y, CWU, and WF. A schematic diagram of the adopted methodology is shown in Fig. 2.

2.6. Estimated variables

The CWU and WF were computed using the calibrated Y model of rainfed and irrigated barley. Crop water use included total evaporative water and water used in transpiration during the period of crop growth. For rainfed barley, CWU was determined by actual evapotranspiration (ET) during the growing season. It was based on green water storage in the soil which is generated by infiltration of the precipitation into the soil. The CWU of the irrigated barley consisted of green CWU, which is based on effective precipitation that forms soil moisture, and blue CWU which is based on irrigated water in the model. The CWU was calculated on a daily basis and aggregated for the growing season (planting to harvesting period).

The WF of the crop was estimated as the ratio of CWU (mm) to Y (t/ha), which is the volume of water consumed per mass production (m^3/t). The total WF for barley consisted of the sum of green and blue. The green WF was calculated based on green CWU, and blue WF was simulated based on blue CWU. In this study, the green WF of barley was calculated for the entire agricultural region (Fig. 1b); while both green and blue WF of irrigated barley were calculated only for irrigated counties (Fig. 1c).

To further adjust and adapt the WF estimates to local water stress conditions in the province, a water stress index (WSI), which is the ratio of total water use by all water use sectors to the blue water resources availability at river basin scale, was calculated and the WF was adjusted. Accounting for local environmental change, i.e., local water stress condition, is important when determining WF, and it reflects the

Table 2
The climate change models used in this study.

GCM name	Institution	Center
CanESM2	Canadian Centre for Climate Modeling and Analysis	CCCma
CCSM4	National Center for Atmospheric Research	NCAR
CNRM-CM5	Centre National de Recherches Meteorologiques/Centre Europeen de Recherche et Formation Avancees en Calcul Scientifique	CNRM-CERFACS
CSIRO-MK5	Commonwealth Scientific and Industrial Research Organization in collaboration with the Queensland Climate Change Centre of Excellence	CSIRO-QCCCE
GFDL-ESM2G	Geophysical Fluid Dynamics Laboratory	NOAA/GFDL
HADGEM2	Met Office Hadley Centre (additional HadGEM2-ES runs by Instituto Nacional de Pesquisas Espaciais)	MOHC (INPE)
MIROC5	Meteorological Research Institute	MIROC
MPI-ESM-LR	Max Planck Institute for Meteorology	MPI-M
MRI-CGCM3	Meteorological Research Institute	MRI

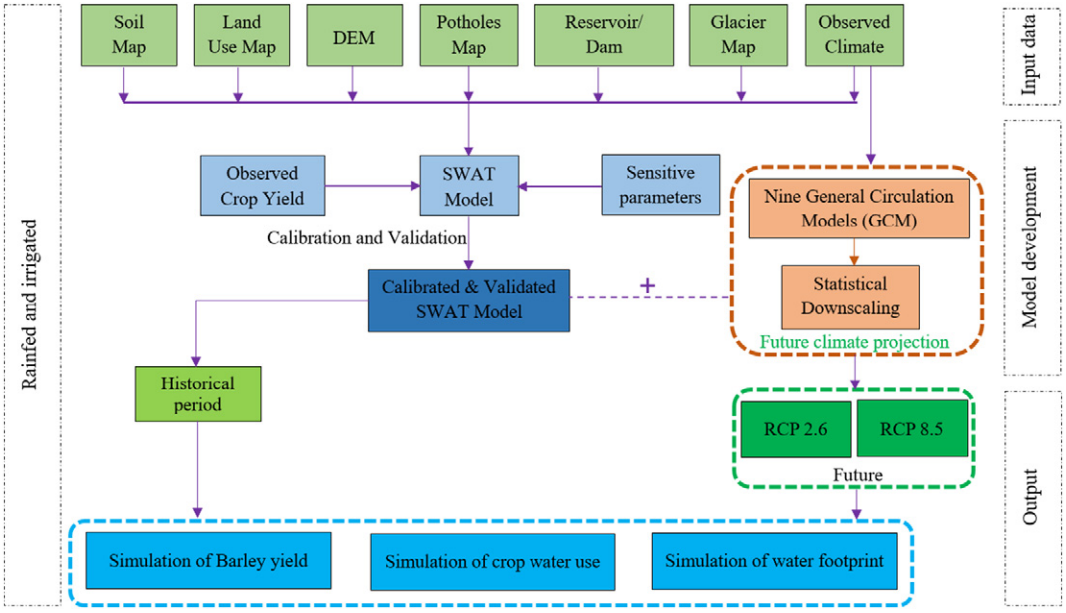

Fig. 2. A schematic diagram of the methodology adopted for this study.

actual local WF status of the region. The WSI was calculated in an earlier study by Faramarzi et al. (2017), where a calibrated hydrologic model of the province was used to account for monthly WSI in 17 major river basins. It was found that southern watersheds suffer from a permanent severe-water stress during summer months. The modified approach of Ridoutt et al. (2012) and Harding et al. (2017) was used in this study to adjust WF to the local WS conditions in different river basins as follow:

$$WF_{adj,RB} = WF \times \frac{WSI_{avg}}{WSI_{thr}} \quad (2)$$

where, $WF_{adj,RB}$ is total WF adjusted to the local water stress conditions in different river basins, WSI_{avg} is the average WSI in the river basin that is calculated based on monthly WSI during crop growing season (May–August), and WSI_{thr} is the threshold of WSI, above which the river basin will be facing severe water stress. A WSI_{thr} of 40% was considered as the threshold level (Faramarzi et al., 2017). Only the WF of the historic period in the irrigated counties was adjusted to the local WSI, since the WSI were computed based on modeled blue water availability from 1985 to 2009 (Faramarzi et al., 2017). For counties that intersected two or more river basins, a weighted area average method was used to adjust the subbasin-based WF into their associated WSI of river basins, then aggregated to the county scale.

3. Results and discussion

3.1. Model set up: Sensitive parameters, calibration, and validation

Sensitivity results of rainfed and irrigated barley in 67 counties, and 11 counties showed that barley Y was sensitive to (1) crop and management related parameters such as DAY, HEAT_UNITS, AUTO_NSTRS, AUTO_NYR, AUTO_EFF, and AUTO_WSTRS; (2) soil-related parameters such as SOL_CBN, SOL_K and SOL_AWC; and (3) parameters related to surface and sub-surface flows such as CN2, EPCO, and ESCO. Definition of these parameters are available in Table 1. As mentioned in Section 2.4, 29 and 32 parameters were initially selected for each rainfed and irrigated county, respectively, based on literature review and author's judgment. Finally, after sensitivity analysis, a total of 805 and 134 parameters were selected for 67 and 11 counties of the rainfed and irrigated barley, respectively.

Fig. 3 shows the calibration and validation results using yearly barley Y data at four counties for both rainfed and irrigated regions for the 1995–2009 and 1983–1994, respectively. The simulated results are expressed at a 95PPU band which is the model output based on a stochastic approach. We do not have a single signal representing model output, rather an envelope of good.

Solutions represented by the 95PPU (Abbaspour, 2015). Larger uncertainty in rainfed barley predicted yields might be due to climate variability and volatile precipitation pattern in Alberta. This has increased standard deviation, as well as thickness of the uncertainty band. As a result a larger r-factor was obtained for rainfed barley. The r-factor was relatively small in irrigated barley, since it is grown under more controlled-stable conditions and natural climate and precipitation fluctuations were mitigated by irrigation. Overall, based on the performance indices during calibration (p-factor, r-factor, and MSE), the rainfed model performed very good (r-factor < 3) in 15 counties followed by good (r-factor < 3–5) in 33 counties and acceptable (r-factor > 5) in 18 counties. Table A1 gives detailed statistics of county-based calibration, validation, and uncertainty analysis data for rainfed barley. In the best performing rainfed counties, the model captured 79% (p-factor 0.79) of observed data with an r-factor of 2.51 and an MSE of 0.54, while in the worst case the model captured 95% (p-factor 0.95) of observed data with an r-factor of 6.85 and an MSE of 0.62. Overall, the provincial average p-factor of rainfed barley was found to be 0.88 and 0.85, with the r-factor of 4.48 and 5.35 for calibration and validation periods, respectively (Table 3).

Table 3 presents the calibration and validation performance for irrigated barley. Overall, 92% (p-factor 0.92) and 82% (p-factor 0.82) of the observed yields were bracketed by 95PPU with an r-factor of 2.13 and 2.34, and MSE of 0.23 and 0.68 for calibration and validation periods, respectively. A moderate uncertainty was found in some counties (Table A2). This inherent uncertainty is frequently encountered in large-scale models due to data errors (e.g., errors in model input data and in reporting yield statistics), process simplification (e.g., large scale semi-physical processes rather than very detail phenological-empirical relationships), and variation in management practices (e.g., differences in crop varieties within a county during calibration and validation periods). Overall, better model performance was obtained for irrigated versus rainfed barley.

As crop Y and CWU (i.e. actual ET) are closely related, our simulated actual ET were further verified through comparison to the estimated actual ET data from Alberta Agriculture and Forestry (AAF). The AAF

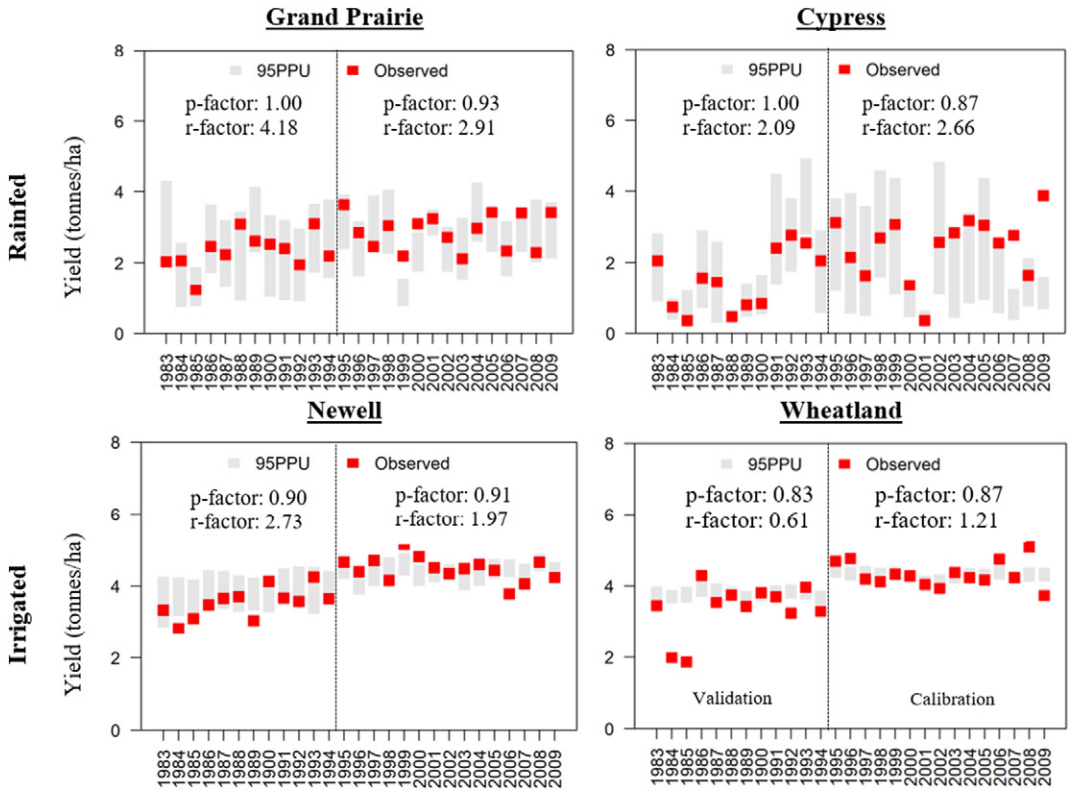

Fig. 3. Comparison of observed and simulated barley yield during calibration (1995–2009) and validation (1983–1994) period for four selected counties growing rainfed and irrigated barley.

estimates are based on the Penman-Monteith method and crop coefficients that applied measured agro-meteorological data at different stations in southern Alberta. The AAF data are available at a seasonal level. For comparison purpose, our simulated ET was aggregated from sub-basin to county scale, likewise, the station-based estimates of AAF were propagated to the county level. In most counties, the estimated ET from AAF were spread within 95PPU band (Fig. A1). The difference of ET in some counties can be explained by the fact that the underlying spatio-temporal resolution of data are not the same. For instance, the AAF data are the maximum and minimum of the available time series for different stations. These time series were not identical for all counties, and some had only 2–3 years of data. Nonetheless, the calibration and validation results and verification of actual ET indicate that our uncertainty-based model is reliable to use for further climate change impact analysis.

3.2. Future climate change scenario results

In this section, the sub-basin based data were aggregated to county level, and spatiotemporal variation of mean precipitation and temperature are discussed. For the agricultural growing season (May–August), mean precipitation for the historical (1985–2009) and future (2040–2064) periods, and their coefficient of variation (CV) are shown in Fig. 4a. As expected, our simulation showed minimum precipitation in the southeast counties of Alberta followed by northwest counties. Maximum precipitation was found in the central portion of the province. Similar spatial patterns were seen in the future period for both RCP 2.6 and 8.5. The spatial pattern of CV showed that there is a substantial fluctuation in the precipitation in southern counties, which was as high as 44% followed by 32% in the northern and 20% in the middle of the province. The projected changes in precipitation indicated a likely increase from 3 to 15%, with the maximum (15%) in the northern and the minimum (3%) in central counties (Fig. 4, right column). However, in the south and south-western counties the precipitation showed a likely decrease by up to 9% as compared to the historical period. The maximum declines were found for the RCP 8.5 in the southwestern part of the province, with large year-to-year fluctuations as indicated by the high CV.

The mean historical temperature varied from 10 to 20 °C with the maximum in south-eastern counties (Fig. 4b). The spatial pattern of mean temperature in the future was found to be similar to historic values, but with larger magnitudes (10 to 22 °C). However, the CV indicated that warmer temperatures in the southern part of the province will be more stable in the future. In the future, temperatures are predicted to increase from 1.4 to 2.3 °C for RCP 2.6, and 2.5 to 3.7 °C for RCP 8.5. The highest temperature changes occurred in southern counties, while the lowest changes were in middle and northern counties. The spatial distribution of CV for both precipitation and temperature (Fig. 4) indicated that the spatiotemporal variability of precipitation is higher than that of temperature.

Table 3
Calibration and validation statistics for rainfed and irrigated barley.

	Rainfed Barley					
	Calibration			Validation		
	p-factor	r-factor	MSE	p-factor	r-factor	MSE
Minimum	0.53	1.91	0.002	0.55	1.65	0.11
Maximum	1.00	8.04	2.10	1.00	8.93	2.30
Average	0.88	4.48	0.60	0.85	5.35	0.59
	Irrigated Barley					
Minimum	0.80	1.21	0.01	0.50	0.61	0.17
Maximum	1.00	3.22	0.61	0.93	3.66	1.90
Average	0.92	2.13	0.23	0.82	2.34	0.68

3.3. Future barley yield projection

The current and future projection of rainfed barley yields showed large differences between the lower and upper 95PPU due to prediction

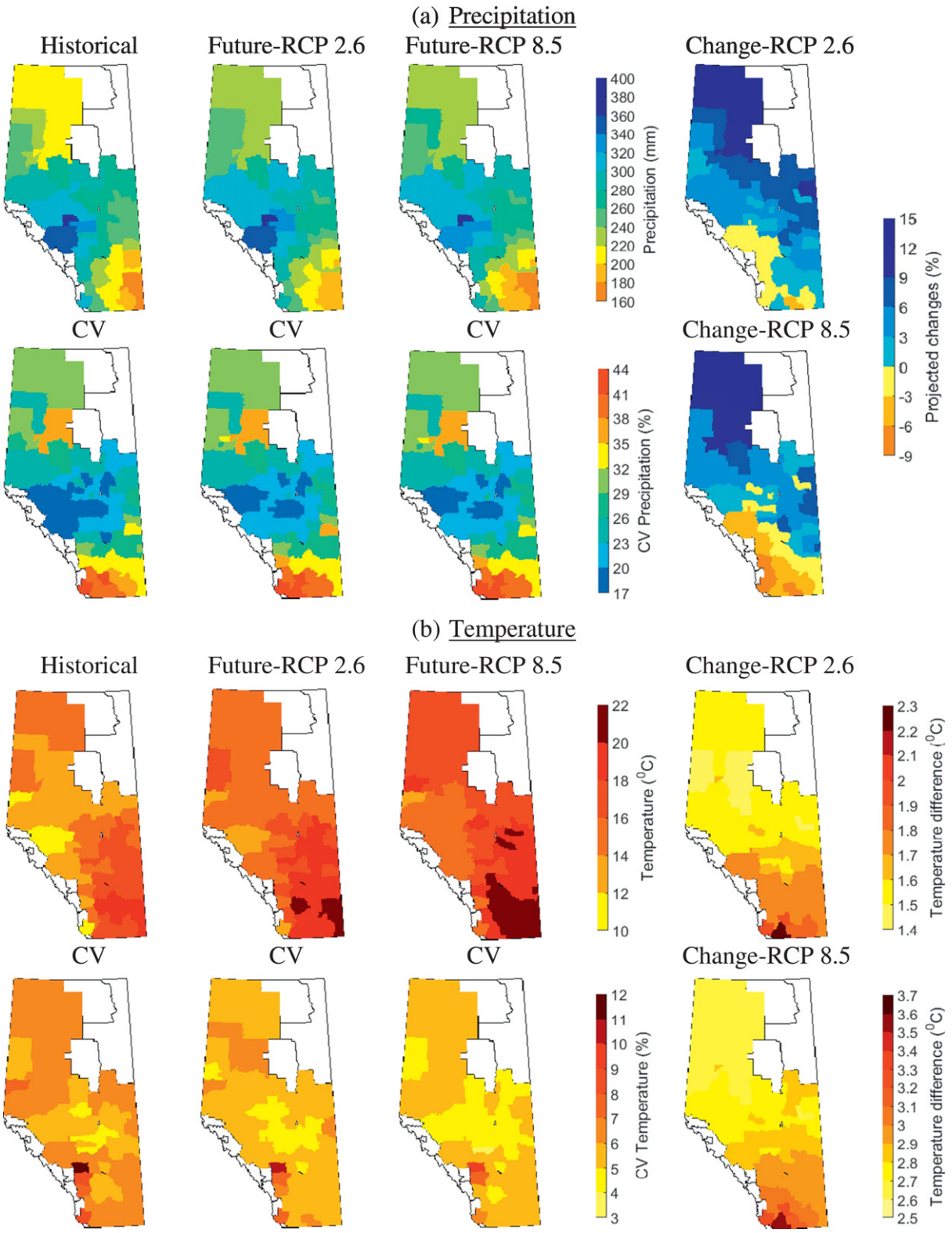

Fig. 4. (a) Mean precipitation and (b) temperature in the historical (1985–2009) and future (2040–2064) periods. The first column in the left shows the historical mean values falling in the growing season (May–August) and their CVs. The second and third columns show similar results but for the future period for RCP 2.6 and 8.5, respectively. The last column in the right shows the projected changes in precipitation (%) and temperature (°C) for the two RCPs.

uncertainties. The 95PPU band of Y showed that maximum yields occur in the northern counties, while minimum yields occur in southern counties (Fig. 5). The spatial pattern in the future projected Y showed that almost the entire province will achieve higher barley yields than in the past. Based on the M95PPU, the Y was projected to increase by up to 80% and 110% for RCP 2.6 and RCP 8.5, respectively (Fig. 5). An increase in precipitation and temperature in the central and northern regions (Fig. 4a,b) will likely contribute to higher Y potential. In the southern part of the province, the increased Y might reflect increased soil moisture, despite the reduced precipitation (Fig. 4a). A soil water

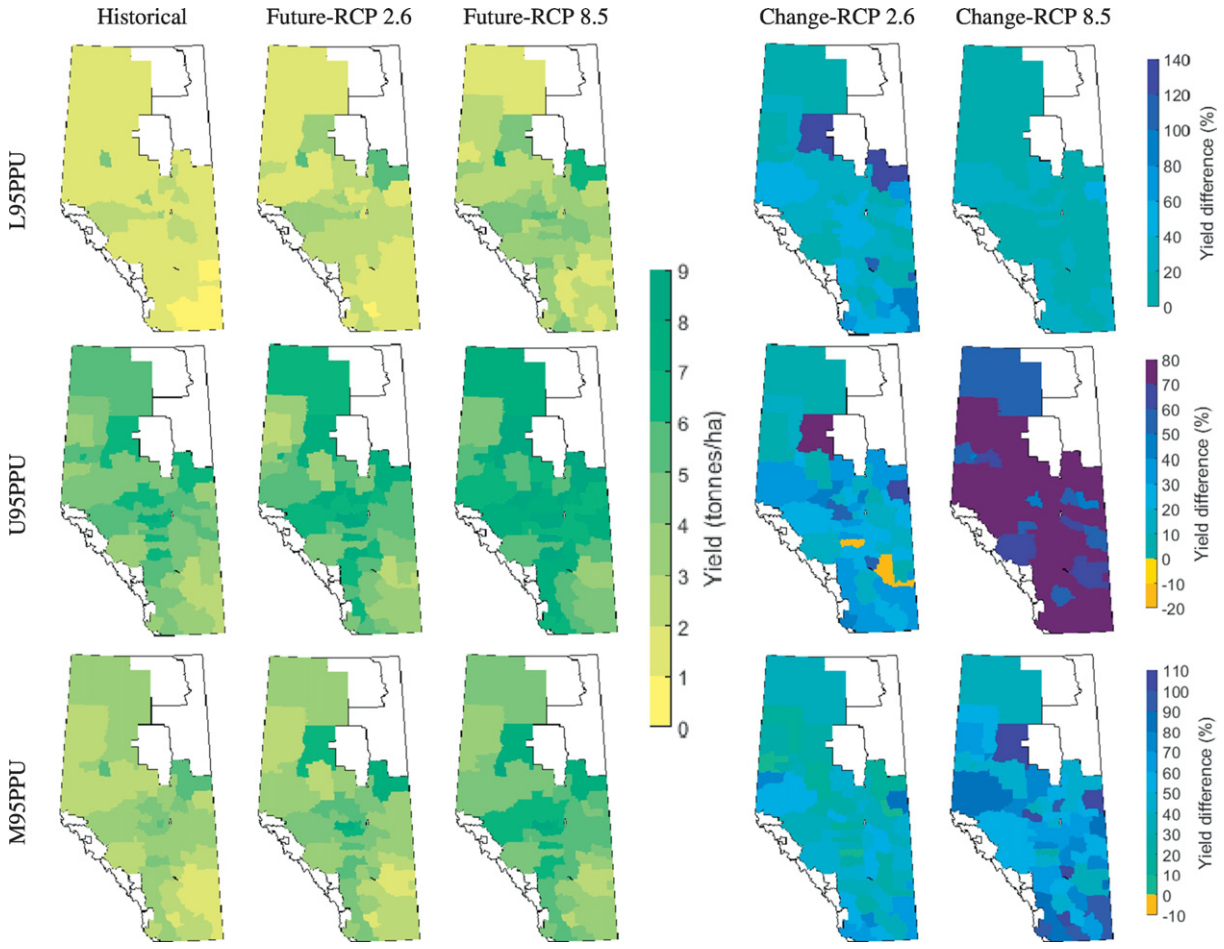

Fig. 5. Model simulated rainfed barley yield (tonnes/ha) for historical and future period and their projected changes (%). Here, L95PPU and U95PPU indicate the lower and upper bound of the model results uncertainty (95PPU). M95PPU indicates the median of the 95PPU band.

balance analysis from our hydrological model (Faramarzi et al., 2015) indicated that soil moisture during the growing season is likely to increase in the southern part of the province (Figs. A3 and A4) as a result of enhanced recharge linked to increased precipitation during the previous fall and winter. Soil moisture during the growing season is highly dependent on fall and winter precipitation in Alberta (Government of Alberta, 2017). Moreover, the increasing trend in atmospheric CO_2 concentration could also explain the overall increase in yields since C3 plant species (e.g. rice, wheat, barley, etc.) react positively to high CO_2 concentrations in the atmosphere (Bocchiola, 2015).

While the rainfed barley Y is predicted to increase in the future, the irrigated barley Y response differed (Fig. 6). The 95PPU band indicates that the projected increase or decrease will be limited to within ±30%. The M95PPU predictions showed that in most counties, the irrigated barley Y is projected to increase or decrease by up to ±5%, which is considered minimal, i.e., unchanged, in large-scale studies due to various uncertainties associated with the Y projection. Theoretically, Y and ET follow a bell-shaped relationship, where an increment in soil water availability will contribute to both productive transpiration (increased T) and non-productive evaporation (E). This will cause an increase in low yields (left side of the bell shape graph, (Fig. 7). Not surprisingly, average rainfed yields (2.4 t/ha) were markedly smaller than irrigated yields (4.7 t/ha). Therefore, increased CO_2 and soil moisture in the future will likely increase rainfed yields, while irrigated yields are likely near the genetic limits of the crop. As such, more soil moisture and irrigation will not result in increased Y. We further explored the possible factors responsible for the decreasing Y in irrigated Taber and Wheatland counties (Fig. 1c). Although precipitation decreased slightly in Taber and increased in Wheatland, soil moisture increased during the month of May and June in both counties. We used plant water demand-based auto irrigation management operation in the model, which aimed at keeping the soil moisture at optimum levels during the growing season. However, this could have no or detrimental effects to yields under certain circumstances. For example, high moisture conditions during crop emergence (i.e., spring) could have negative impacts on root development, restricting the rooting depth to the top layers of the soil profile and compromising plant development during the remainder of the growing season, despite irrigation. This aspect has been discussed by Cordeiro et al. (2015) for corn grown under wet spring conditions in Manitoba. Irrigation events followed by excess precipitation during this period could exacerbate the problem. The spatial pattern of water and temperature stress days are provided in Fig. A2 and were predicted to decrease in both irrigated and rainfed crops.

3.4. Future CWU projection

The CWU is the actual evapotranspiration (AET), which is the total amount of water transpired (T) and evaporated (E) from the plant and soil surface during the growing season. The modeled L95PPU and U95PPU of CWU in rainfed barley varied from 80 mm to 390 mm during the historical period (Fig. 8). Using the M95PPU, the CWU varied from 130 mm to 350 mm across the province. The spatial pattern of future CWU was similar to the historical, however, with different magnitudes. Overall, a decrease in CWU was predicted as RCP moved from 2.6 to 8.5. The M95PPU projections showed that CWU will decrease in northwestern counties, while in southern and southeastern counties it will increase.

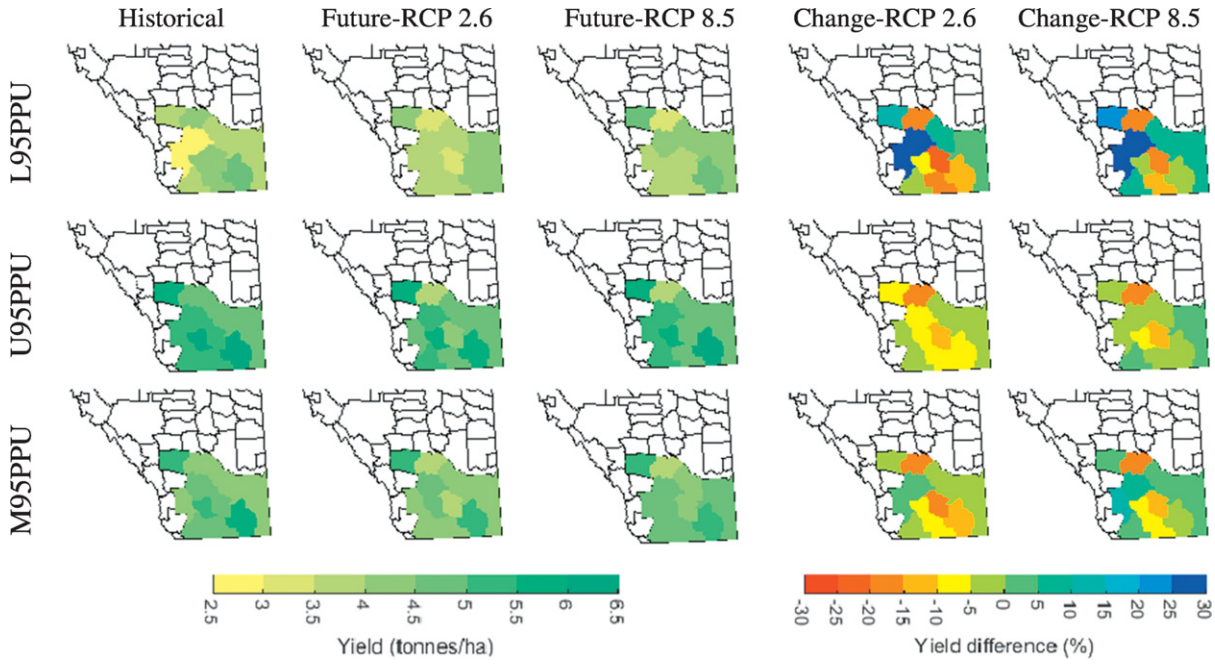

Fig. 6. Model simulated irrigated barley Y (tonnes/ha) for historical and future period and their projected changes (%). Here, L95PPU and U95PPU indicate the lower and upper bound of the model results uncertainty (95PPU). M95PPU indicates the median of the 95PPU band.

Overall the simulated CWU of the irrigated barley was substantially higher than that of rainfed barley in both historic and future periods. A higher CWU in irrigated barley is expected because of more soil water availability that contributes to evapotranspiration in favor of biomass and Y production. However, the spatial decreasing trend is similar to the rainfed barley. Using simulated M95PPU, the historical values ranged from 380 mm to 580 mm, while it varied from 260 mm to 540 mm in the future with most counties falling in the lower range under the RCP 8.5 scenario (Fig. 9). The ensemble model projected a decreasing rate of CWU in the future for both RCPs. As mentioned earlier, the principal response of barley to increasing CO_2 concentration is to reduce transpirational water loss by decreasing stotamal conductance (Ainsworth and Rogers, 2007; Lammertsma et al., 2011). Therefore, a lower CWU is projected with reduced or similar Y in irrigated counties due to CO_2 effects, although temperature is projected to increase in the southern Alberta. This response is visible through the monthly variation of actual ET in Taber and Wheatland county (Fig. A4), where actual ET decreases in July and August given >1 °C and >3 °C temperature rise for RCP 2.6 and 8.5, respectively. Similar results have been found in the San Luis Valley of Colorado (Ramirez and Bryce, 1996). Results from their study revealed that the CO_2 induced effects on PET are greater than those induced by temperature change, with the combination of 3 °C increase in temperature and a doubling of CO_2 resulting in an 18.5% decrease in PET. A detailed analysis of the blue and green CWU in irrigated barley found that all of the irrigated counties would likely observe an increase in green CWU (Fig. 10a). However, this increasing pattern did not mimic projected precipitation in Fig. 4a, but did align with changes in soil moisture (Fig. A3). In contrast to green CWU, our model projected a reduction in blue CWU for irrigated barley (Fig. 10b), as the model assumes that crops will be irrigated as soon as water demand exceeds supply. Therefore, the proportion of green CWU is higher than blue CWU and in turn, green CWU increases and blue CWU decreases.

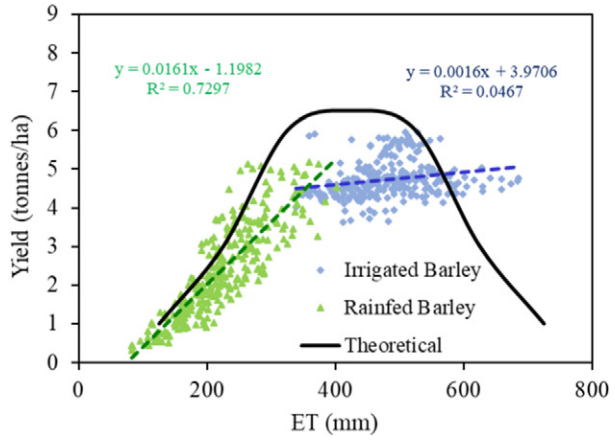

Fig. 7. Simulated Y and ET relationship for irrigated and rainfed barley crops for historical period (1986–2009). M95PPU values of yearly outputs are used for simulated graphs. Theoretical line is based on assumed numbers.

3.5. Future water footprint projection

The spatial distribution of WF of rainfed barley is illustrated in Fig. 11a. Using M95PPU, the range of water footprint varied from 200 to 1300 m^3/t from southern to northern Alberta in both historical and future periods. The model showed that WF is likely to decrease in the future and from scenario RCP 2.6 to RCP 8.5. This might be a reflection of complex interactions between CO_2, precipitation, temperature, water, and Y. Under the worst-case scenario of RCP 8.5, the total WF (green + blue) of irrigated barley would be smaller than rainfed barley. Based on changes in all contributing factors, a decreased WF of irrigated barley may not be in favor of increased crop Y, but could result in reduced blue CWU in the future. Depending on the scenario, only 200–700 m^3 of water would be required to produce a tonne of barley under rainfed condition in northern Alberta (Fig. 11a). However, 600–1100 m^3 of water would be needed for the same production in irrigated barley in southern Alberta (Fig. 11b). The M95PPU for rainfed and irrigated barley is tabulated in Table A3 and A4 in the Supplementary material.

Similar to rainfed barley, the WF for irrigated barley will likely decrease in the future. However, there are some counties where water footprint will increase under scenario RCP 2.6, whereas the blue WF may decrease in the future (Fig. 12). Moreover, the green WF was predicted to increase in both RCP 2.6 and RCP 8.5 scenarios. Our results suggested

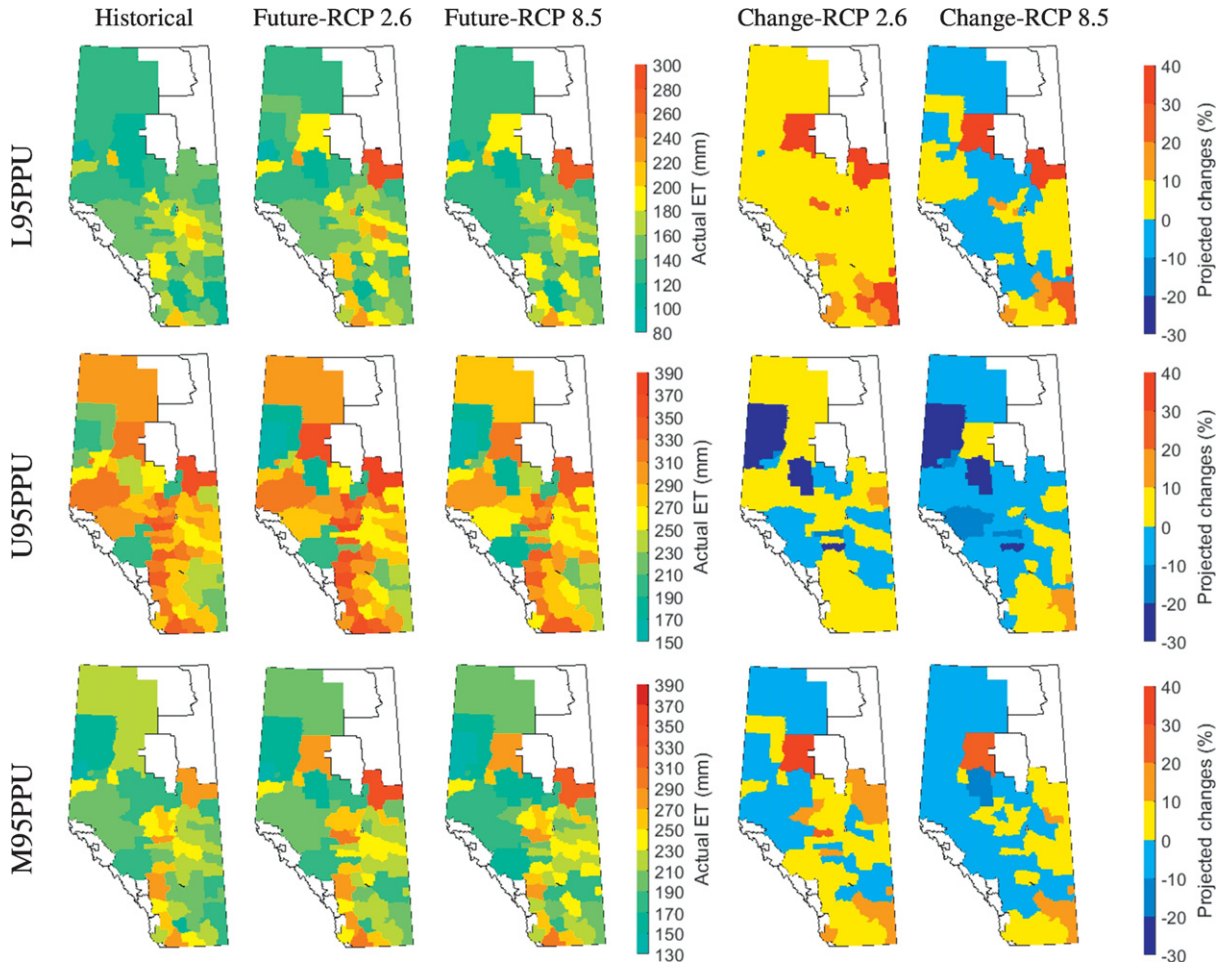

Fig. 8. Spatial pattern of CWU for the rainfed barley and their projected changes. Here, L95PPU and U95PPU indicate the lower and upper bound of the model results uncertainty (95PPU). M95PPU indicates the median of the 95PPU band.

a decreased WF align with an increased CWP, i.e. an increased production per unit of water consumption. This might be seen as an opportunity to cope with likely water stress conditions during the summer months (July–August, Faramarzi et al., 2017). Sun et al. (2012) studied the impact of climate change on the WF of wheat in an irrigation district in China. They found a decrease in crop evapotranspiration, accompanied by increasing Y, resulting in a decreased WF. Our results can also be supported by the work of Shrestha et al. (2017a) where they studied impact of climate change on the Y and WF of rice in the Nam Oon irrigation project in Thailand. The results indicated that dry rice Y (variety ChaiNat-1) is likely to increase and the WF decrease as precipitation will decrease.

3.6. Water stress adjusted WF

The adjusted WF of irrigated barley for historic period indicated that in the best case WF was 542 m^3 in Cypress County. The Cypress County is located is spread within Red Deer River Basin with a WSI of about 8.96%, and Bow River Basin with a WSI of about 50.25% (Table 4). However, without consideration of water stress, the WF was estimated to be 1130 m^3 in this county. The simulated WF was 1359 m^3 in Willow Creek within the Oldman River Basin (WSI ≈ 52.36%), which decreased to 1038 m^3 in the absence of water stress. As already mentioned, counties that intersected two river basins, a weighted area average method was used to adjust the subbasin-based WF into their associated WSI of river basins, then aggregated to the county scale. Overall, the stress adjusted WF of all irrigated counties was 12,200 m^3, while the unadjusted WF was 11,010 m^3. The adjusted WF to the watershed-based WSI resulted in a total of 2194 m^3 (~20%) increase in 8 counties, and a total 918 m^3 (~9%) decrease in 3 counties (Table 4). It is noteworthy that current WF_{adj} values might be underestimated, since downstream water needs of Alberta (e.g. transboundary water treaties with the Province of Saskatchewan) were not accounted for. Some other emerging water needs, namely urbanization, industrialization and fracking also could modify the WF_{adj} values. Assessing the WSI in the future will require both water supply and demand assessment of the watersheds. Therefore, WF_{adj} values were computed only for the historic period and the framework developed in this study can be applied for the WF_{adj} accounting of future projections.

We compared our results with the literature (e.g., Mekonnen and Hoekstra, 2011, 2014), where they summarized WF of various crops across the world. Since these studies relate to dissimilar climate and soil conditions and management practices, the WF values for a given crop vary over a wide range. For instance, Mekonnen and Hoekstra (2014) established a set of global WF benchmark values for a large number of crops grown in the world including barley. They found that WF (blue and green WF) of barley in the Canadian prairies, which includes southern Alberta, is 546–1029 m^3/t. Whereas, our study found that the WF of barley in southern Alberta (irrigated counties) varies from 767 to 1269 m^3/t (unadjusted and based on M95ppu, Table 4). Besides, the adjusted WF range from 542 to 1661 m^3/t in the presence of water stress conditions. This is an indication that disregarding the regional conditions are not representative enough and the results from such studies could be misleading and may negatively impact decision on regional, national and global water management and food trade policies.

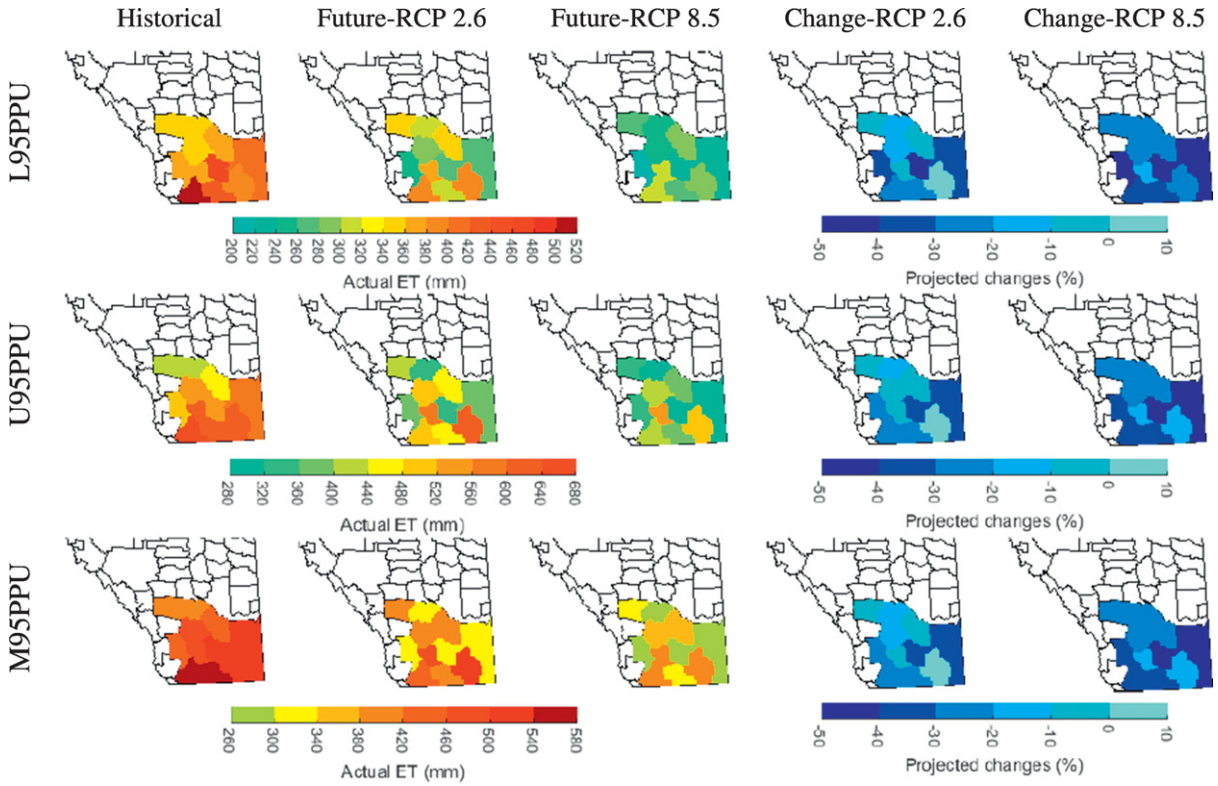

Fig. 9. Spatial pattern of CWU for the irrigated barley and their projected changes. Here, L95PPU and U95PPU indicate the lower and upper bound of the model results uncertainty (95PPU). M95PPU indicates the median of the 95PPU band.

4. Conclusions

The Soil and Water Assessment Tool (SWAT) is used to evaluate the impact of climate change on yield (Y), consumptive water use (CWU) and water footprint (WF) of rainfed and irrigated barley in Alberta, Canada.

The future growing seasonal mean precipitation is projected to increase in central to northern Alberta with low spatial variability but is projected to decrease in southern Alberta with high spatial variability. The maximum projected increase in seasonal precipitation is 15% in the north, while the maximum reduction is 9% in south and southwestern Alberta. The future growing seasonal temperature is projected to increase from 1.4 to 3.7 °C with maximum increases in the south and minimum increases in the north.

Climate change is predicted to lead to an increase in rainfed barley Y throughout Alberta. On the contrary, the irrigated barley Y in southern Alberta is projected to remain unchanged in most of the counties. The yield-evapotranspiration (Y-ET) relationship in the rainfed and irrigated

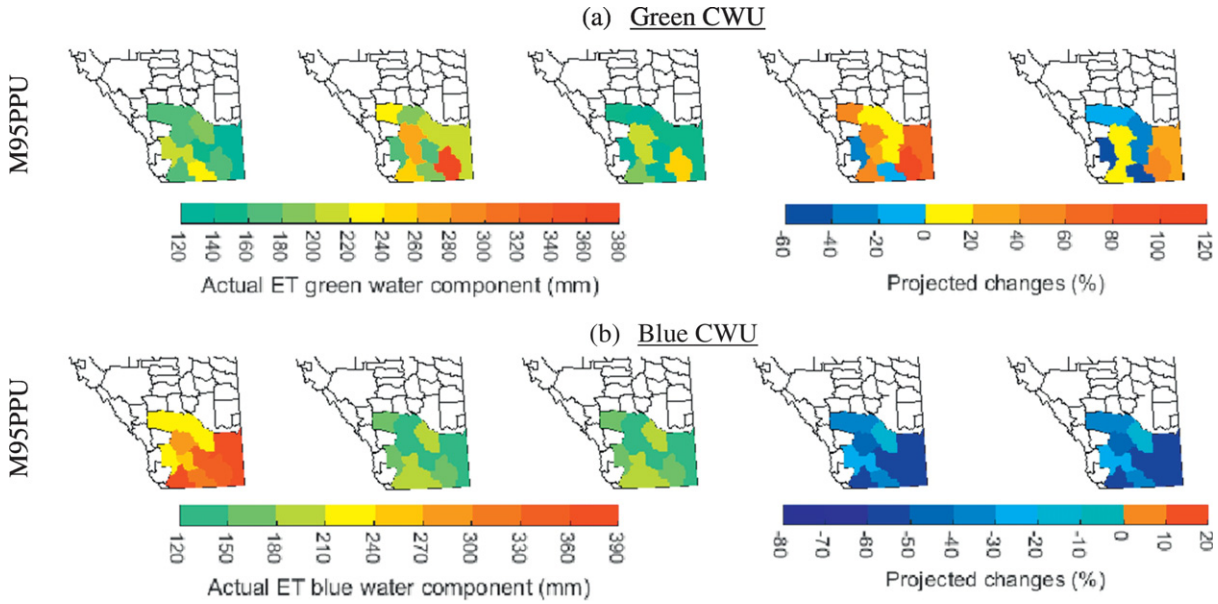

Fig. 10. Spatial distribution of (a) green and (b) blue CWU for irrigated barley and their projected changes. Here, M95PPU indicates the median of the 95PPU band.

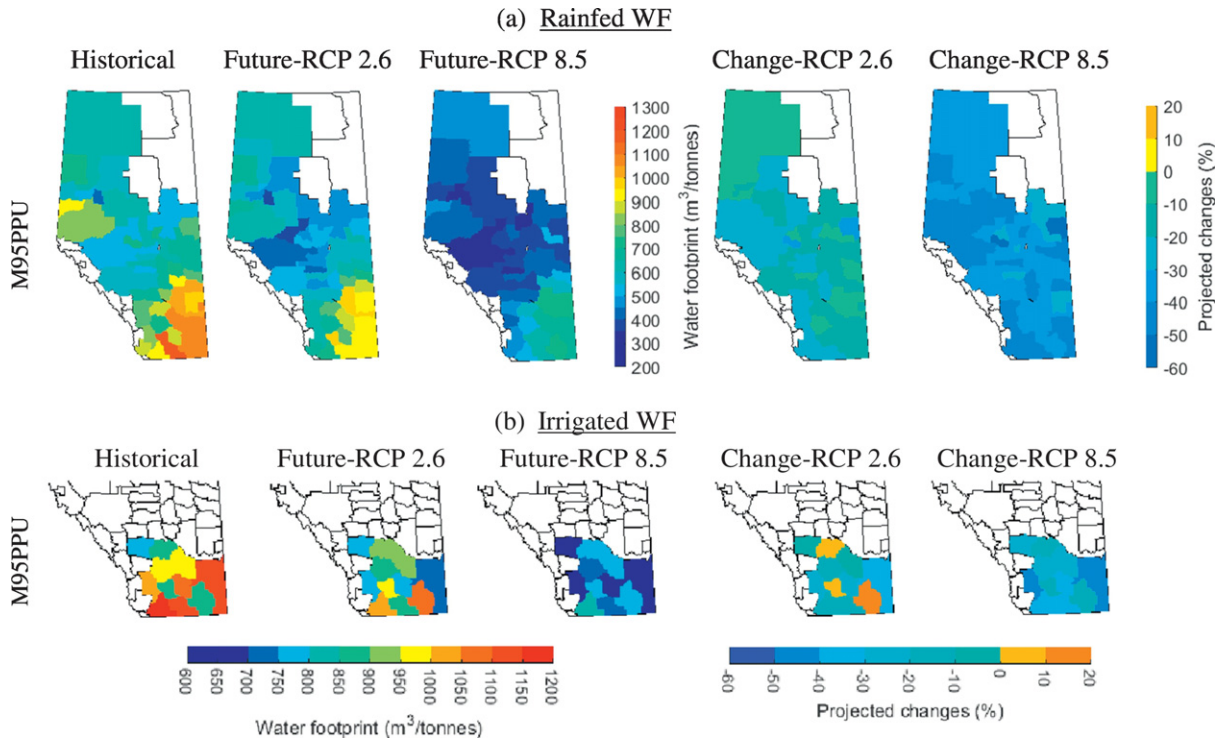

Fig. 11. Spatial pattern of WF for the (a) rainfed and (b) irrigated barley and their projected changes. Here, M95PPU indicates the median of the 95PPU band.

regions showed that future increases in CO_2 and soil moisture will likely increase rainfed yields, while irrigated yields are projected to reach their genetic limits.

The CWU for rainfed and irrigated agriculture is predicted to decrease in most counties, indicating that less water will be required for barley production in the future. The decreasing trend of rainfed CWU agrees well with the precipitation pattern and effective rainfall in the north, while it mimics soil moisture pattern due to earlier snow melt in southern counties. The analysis of blue and green CWU in the irrigated counties revealed that in the future green water is likely to satisfy a greater proportion of crop demands than blue water.

Considering the impact of climate change, WF will decrease in the future as a result of higher barley Y and lower CWU due to complex interactions between CO_2, precipitation, temperature, soil moisture, and Y. Based on the results of WF analysis, higher amounts of water will be required to produce a tonne of barley in southern (irrigated) than in

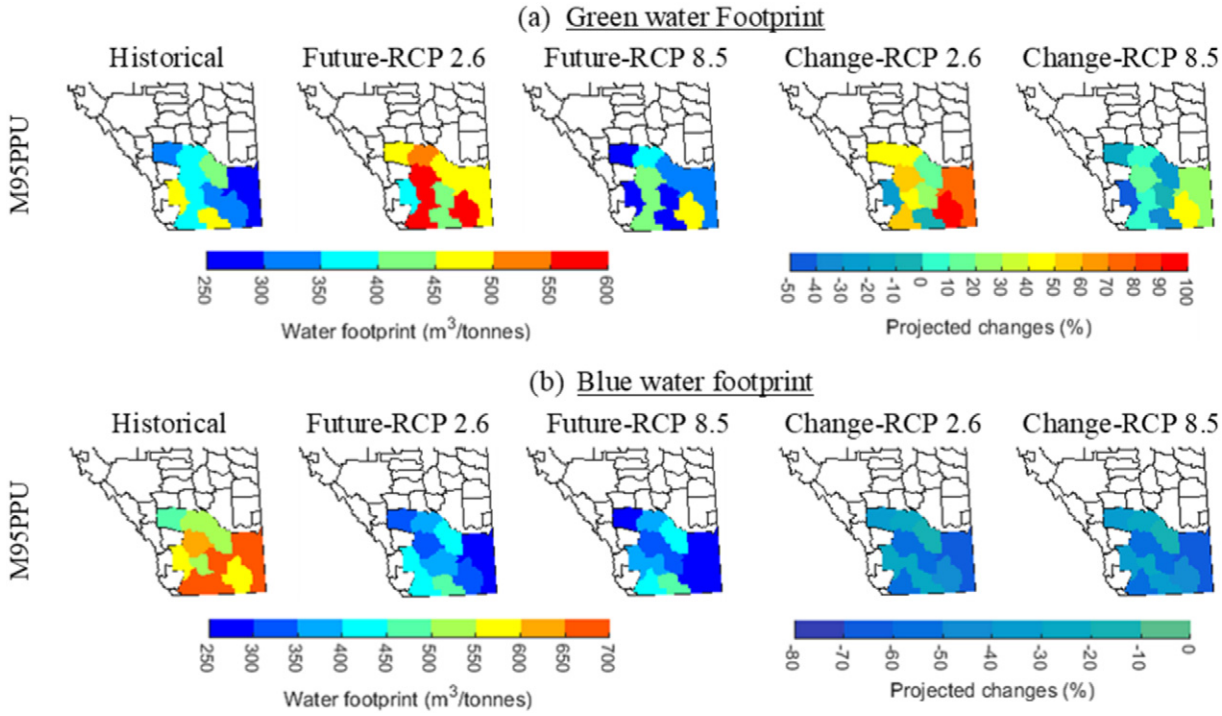

Fig. 12. Spatial pattern of (a) Green and (b) Blue water footprint for the irrigated barley and their projected changes. Here, M95PPU indicates the median of the 95PPU band.

Table 4
Comparison of the simulated water footprint (WF) and the location adjusted WF (WF_{adj}) of irrigated barley to the watershed level WSI for the historic period. Counties with reduced water footprint after adjusting to local WSI are shaded with grey.

County	L95PPU-U95PPU		M95PPU	
	WF	WF_{adj}	WF	WF_{adj}
Cardston	1462–1267	1915–1658	1269	1661
Cypress	1064–1179	510–566	1130	542
Forty Mile	791–952	645–776	892	727
Lethbridge	948–990	1241–1296	897	1174
Newell	998–983	1248–1229	971	1214
Rocky View	946–725	1183–907	767	959
Taber	1063–1055	1392–1381	1051	1375
Vulcan	1231–1005	1575–1286	993	1270
Warner	1015–1202	1167–1382	1120	1288
Wheatland	847–901	624–664	882	650
Willow Creek	1354–971	1772–1271	1038	1359

northern (rainfed) Alberta. Spatially, the minimum WF would be observed in the western counties as compared to central and eastern counties. Considering local water stress condition, the adjusted WF of irrigated barley indicated a considerable reduction in WF in Cypress, Forty Mile, and Wheatland counties, while it increased in all other irrigated counties.

Overall, our locally adapted regional model through advanced computing systems, allowed to better utilize hydrologic and crop growth models to improve WF data quality by providing more reliable, and higher spatial and temporal resolution as compared to the global models that lack consideration of local agro-hydrological data. In addition, most of the regional studies on WF are conducted for the past and the present time, and the policy options and challenges to improve water use pattern are discussed for the status-quo situation (Yang et al., 2013). Our WF projections under various climate change scenarios contribute to advance the knowledge on future water opportunities, e.g. reduced WF, in this globally important agricultural region. This helps to facilitate the development of local and global future water policies in support of the sustainable economy and improved human and environmental well-being.

4.1. Caveats

The modeling tool and research framework we built here will provide a way to investigate the potential adaptation strategies under future climate scenarios. However, similar to other process-based models, our work might have some conceptual errors and tenuous assumptions. For example, we did not consider the impact of crop rotation, pesticides or herbicides, manure application, all of which may contribute to the uncertainty of crop yields. We also assumed wind speed and relative humidity would remain unchanged in the future. Regarding the auto irrigation and auto fertilizer application management operations, one would have to verify that they are reflective of actual on-farm management practices. In addition, we have considered baseline agricultural management operation for the future projections, i.e. fertilizer application, tillage operation, plating and harvest/kill timing assumed unchanged in our future scenarios. Further research is needed to assess trade-offs between natural and agricultural management factors on optimal Y, CWU, and WF_{adj}.

Moreover, our projections of regional WF was based on the agro-hydrologic models that were calibrated to replicate longest possible historical Y data. Similar to other modeling studies, we calibrated based on 'near-term' observed records that are based on the assumption that climate and hydrology fluctuate within a constant range of variability, so-called stationarity (Gray and McCabe, 2010). However, recent studies revealed shifts in the degree of variability in climate regimes that exceed the length of instrumental records, and are not adequately represented in both climate change and hydrologic model simulations (Sauchyn et al., 2015). Further research is needed to integrate such large-scale variabilities in both climate change and agro-hydrologic models.

Acknowledgement

We gratefully acknowledge the funding from Alberta Livestock and Meat Agency of the Alberta Agriculture and Forestry (Grant #2016E017R). We wish to thank Alberta Financial Service Corporation for providing the crop Y data. We also would like to thank the anonymous referees for providing insightful suggestions to improve the paper.

Appendix A. Supplementary data

Supplementary data to this article can be found online at https://doi.org/10.1016/j.scitotenv.2017.11.004.

References

Abbaspour, K., 2015. SWAT-Calibration and Uncertainty Programs (CUP). Neprashtechnology.Ca. https://doi.org/10.1007/s00402-009-1032-4.
Abbaspour, K.C., Yang, J., Maximov, I., Siber, R., Bogner, K., Mieleitner, J., Zobrist, J., Srinivasan, R., 2007. Modelling hydrology and water quality in the pre-alpine/alpine Thur watershed using SWAT. J. Hydrol. 333:413–430. https://doi.org/10.1016/j.jhydrol.2006.09.014.
Abbaspour, K.C., Rouholahnejad, E., Vaghefi, S., Srinivasan, R., Yang, H., Kløve, B., 2015. A continental-scale hydrology and water quality model for Europe: calibration and uncertainty of a high-resolution large-scale SWAT model. J. Hydrol. 524:733–752. https://doi.org/10.1016/j.jhydrol.2015.03.027.
Ahuja, L.R., Andales, A.A., Ma, L., Saseendran, S.A., 2007. Whole-system integration and modeling essential to agricultural science and technology for the 21st century. J. Crop. Improv. 19 (1–2):73–103. https://doi.org/10.300/J411v19n01_04.
Ainsworth, E.A., Rogers, A., 2007. The response of photosynthesis and stomatal conductance to rising [CO2]: mechanisms and environmental interactions. Plant Cell Environ. 30:258–270. https://doi.org/10.1111/j.1365-3040.2007.01641.x.
Alberta Agriculture, Rural Development, 2004. Alberta fertilizer guide. URL. http//:www1.agric.gov.ab.ca/$department/deptdocs.nsf/all/agdex3894/$file/541-1.pdf, Accessed date: 15 September 2016.
Alberta Cattle Feeders' Association, 2017. Facts and Stats – Alberta Cattle Feeders Association. URL http://www.cattlefeeders.ca/industry-overview/alberta-cattle-feeding-facts-and-stats/, Accessed date: 16 March 2017.
Alberta WaterPortal, 2017. Agriculture and Irrigation in Alberta. URL. http://albertawater.com/what-is-water-used-for-in-alberta/agriculture-in-alberta, Accessed date: 4 October 2017.
Allen, R.G., Jensen, M.E., Wright, J.L., Burman, R., 1989. Operational estimates of reference evapotranspiration. Agron. J. 81, 650–662.
Arnold, J.G., Srinivasan, R., Muttiah, R.S., Williams, J.R., 1998. Large area hydrologic modeling and assessment part I: model development. J. Am. Water Resour. Assoc. 34:73–89. https://doi.org/10.1111/j.1752-1688.1998.tb05961.x.
Azimi, M., Heshmati, G.A., Farahpour, M., Faramarzi, M., Abbaspour, K.C., 2013. Modeling the impact of rangeland management on forage production of sagebrush species in arid and semi-arid regions of Iran. Ecol. Model. 250:1–14. https://doi.org/10.1016/j.ecolmodel.2012.10.017.
Basheer, A.K., Lu, H., Omer, A., Ali, A.B., Abdelgader, A.M.S., 2016. Impacts of climate change under CMIP5 RCP scenarios on the streamflow in the Dinder River and ecosystem habitats in Dinder National Park, Sudan. Hydrol. Earth Syst. Sci. 20:1331–1353. https://doi.org/10.5194/hess-20-1331-2016.
Beven, K., Binley, A., 1992. The future of distributed models: model calibration and uncertainty prediction. Hydrol. Process. 6:279–298. https://doi.org/10.1002/hyp.3360060305.
Bocchiola, D., 2015. Impact of potential climate change on crop yield and water footprint of rice in the Po valley of Italy. Agric. Syst. 139:223–237. https://doi.org/10.1016/j.agsy.2015.07.009.
Cannon, A.J., 2015. Selecting GCM scenarios that span the range of changes in a multimodel ensemble: application to CMIP5 climate extremes indices. J. Clim. 28, 1260–1267.
Chen, J., Brissette, F.P., Leconte, R., 2011. Uncertainty of downscaling method in quantifying the impact of climate change on hydrology. J. Hydrol. 401:190–202. https://doi.org/10.1016/j.jhydrol.2011.02.020.
Cordeiro, M.R.C., Krahn, V., Ranjan, R.S., Sager, S., 2015. Water table contribution and diurnal water redistribution within the corn root zone. Can. Biosyst. Eng. 57, 39–48.
FAO (Food and Agriculture Organization of the United Nations), 2017. How to Feed the World in 2050. URL. http://www.fao.org/fileadmin/templates/wsfs/docs/expert_paper/How_to_Feed_the_World_in_2050.pdf, Accessed date: 18 October 2017.
Faramarzi, M., Yang, H., Schulin, R., Abbaspour, K.C., 2010. Modeling wheat yield and crop water productivity in Iran: implications of agricultural water management for wheat production. Agric. Water Manag. 97:1861–1875. https://doi.org/10.1016/j.agwat.2010.07.002.
Faramarzi, M., Srinivasan, R., Iravani, M., Bladon, K.D., Abbaspour, K.C., Zehnder, A.J.B., Goss, G.G., 2015. Setting up a hydrological model of Alberta: data discrimination analyses prior to calibration. Environ. Model. Softw. 74:48–65. https://doi.org/10.1016/j.envsoft.2015.09.006.

Faramarzi, M., Abbaspour, K.C., Adamowicz, W.L., Lu, W., Fennell, J., Zehnder, A.J.B., Goss, G.G., 2017. Uncertainty based assessment of dynamic freshwater scarcity in semi-arid watersheds of Alberta, Canada. J. Hydrol. Reg. Stud. 9:48–68. https://doi.org/10.1016/j.ejrh.2016.11.003.

Farm Credit Canada, 2012. Beef facts. available at:. https://www.fccfac.ca/fcc/agKnowledge/publications/ag-sector-guides/pdfs/beeffacts.pdf, Accessed date: 15 September 2016.

Government of Alberta, Alberta Agriculture and Forestry, Policy and Environment Division, Environmental Stewardship Branch, Engineering and Climate Services Section, 2017. Agroclimatic Atlas of Alberta: soil moisture conditions in Alberta. http://www1.agric.gov.ab.ca/$department/deptdocs.nsf/all/sag6302, Accessed date: 26 July 2017.

Gray, S.T., McCabe, G.J., 2010. A combined water balance and tree ring approach to understanding the potential hydrologic effects of climate change in the central Rocky Mountain region. Water Resour. Res. 46 (W05513).

van Griensven, A., Meixner, T., 2006. Methods to quantify and identify the sources of uncertainty for river basin water quality models. Water Sci. Technol. 53, 51–59.

Grusson, Y., Sun, X., Gascoin, S., Sauvage, S., Raghavan, S., Anctil, F., Sáchez-Pérez, J.-M., 2015. Assessing the capability of the SWAT model to simulate snow, snow melt and streamflow dynamics over an alpine watershed. J. Hydrol. 531:574–588. https://doi.org/10.1016/j.jhydrol.2015.10.070.

Harding, G., Courtney, C., Russo, V., 2017. When geography matters. A location-adjusted blue water footprint of commercial beef in South Africa. J. Clean. Prod. 151:494–508. https://doi.org/10.1016/j.jclepro.2017.03.076.

Hoekstra, A.Y., Chapagain, A.K., Aldaya, M.M., Mekonnen, M.M., 2011. The Water Footprint Assessment Manual. Earthscan Ltd., Dunstan House, 14a St Cross Street, London EC1N 8XA, UK.

IPCC, 2014. Annex II: glossary. In: Mach, K.J., Planton, S., von Stechow, C. (Eds.), Cli- mate Change 2014: Synthesis Report. Contribution of Working Groups I, II and III to the Fifth Assessment Report of the Intergovernmental Panel on Climate Change [Core Writing Team, R.K. Pachauri and L.A. Meyer (Eds.)]. IPCC, Geneva, Switzerland, pp. 117–130.

Islam, Z., Gan, T.Y., 2014. Effects of climate change on the surface-water management of the South Saskatchewan River Basin. J. Water Resour. Plan. Manag. 140 (3), 332–342.

Jiang, R., Gan, T.Y., Xie, J., Wang, Ni., Kuo, C.-C., 2017. Historical and potential changes of precipitation and temperature of Alberta subjected to climate change impact: 1900–2100. Theor Appl. Clim. 127:725–739. https://doi.org/10.1007/s00704-015-1664-y.

Lammertsma, E.I., Jan De Boer, H., Dekker, S.C., Dilcher, D.L., Lotter, A.F., Wagner-Cremer, F., 2011. Global CO_2 rise leads to reduced maximum stomatal conductance in Florida vegetation. PNAS 108:4035–4040. https://doi.org/10.1073/pnas.1100371108.

Legesse, G., Ominski, K.H., Beauchemin, K.A., et al., 2017. Quantifying water use in ruminant production. J. Anim. Sci. 95:2001–2018. https://doi.org/10.2527/jas2017.1439.

Liu, M., He, B., Lü, a., Zhou, L., Wu, J., 2014. Parameters sensitivity analysis for a crop growth model applied to winter wheat in the Huanghuaihai Plain in China. Geosci. Model Dev. Discuss. 7:3867–3888. https://doi.org/10.5194/gmdd-7-3867-2014.

Liu, W., Yang, H., Liu, J., Azevedo, L.B., et al., 2017. Global assessment of nitrogen losses and trade-offs with yields from major crop cultivations. Sci. Total Environ. 572:526–537. https://doi.org/10.1016/j.scitotenv.2016.08.093.

Ma, X., Ma, Y., 2017. The spatiotemporal variation analysis of virtual water for agriculture and livestock husbandry: a study for Jilin Province in China. Sci. Total Environ. 586: 1150–1161. https://doi.org/10.1016/j.scitotenv.2017.02.106.

Marano, R.P., Filippi, R.A., 2015. Water footprint in paddy rice systems. Its determination in the provinces of Santa Fe and Entre Ríos, Argentina. Ecol. Indic. 56:229–236. https://doi.org/10.1016/j.ecolind.2015.03.027.

Masud, M.B., Khaliq, M.N., Wheater, H.S., 2015. Analysis of meteorological droughts for the Saskatchewan River Basin using univariate and bivariate approaches. J. Hydrol. 522: 452–466. https://doi.org/10.1016/j.jhydrol.2014.12.058.

Masud, M.B., Soni, P., Shrestha, S., Tripathi, N.K., 2016. Changes in climate extremes over North Thailand, 1960–2099. J. Climatol. 2016:1–18. https://doi.org/10.1155/2016/4289454.

Maurer, E.P., Hidalgo, H.G., 2008. Utility of daily vs. monthly large-scale climate data: an intercomparison of two statistical downscaling methods. Hydrol. Earth Syst. Sci. 12: 551–563. https://doi.org/10.5194/hess-12-551-2008.

Mckay, M.D., Beckman, R.J., Conover, W.J., 1979. A comparison of three methods for selecting values of input variables in the analysis of output from a computer code. Technometrics 21.

Mekonnen, M.M., Hoekstra, A.Y., 2011. The green, blue and grey water footprint of crops and derived crop products. Hydrol. Earth Syst. Sci. 15:1577–1600. https://doi.org/10.5194/hess-15-1577-2011.

Mekonnen, M.M., Hoekstra, A.Y., 2014. Water footprint benchmarks for crop production: a first global assessment. Ecol. Indic. 46:214–223. https://doi.org/10.1016/j.ecolind.2014.06.013.

Neitsch, S.L., Arnold, J.G., Kiniry, J.R., Williams, J.R., 2011. Soil and Water Assessment Tool Theoretical Documentation Version 2009.

Palazzoli, I., Maskey, S., Uhlenbrook, S., Nana, E., Bocchiola, D., 2015. Impact of prospective climate change on water resources and crop yields in the Indrawati basin, Nepal. Agric. Syst. 133:143–157. https://doi.org/10.1016/j.agsy.2014.10.016.

Prowse, T.A.A., Bradshaw, C.J.A., Delean, S., Cassey, P., Lacy, R.C., Wells, K., Aiello-Lammens, M.E., Akçakaya, H.R., Brook, B.W., 2016. An efficient protocol for the global sensitivity analysis of stochastic ecological models. Ecosphere 7, e01238. https://doi.org/10.1002/ecs2.1238.

Ramirez, J., Bryce, F., 1996. CO_2 and temperature effects on evapotranspiration and irrigated agriculture. J. Irrig. Drain. Eng. 155–163.

Ridoutt, B.G., Sanguansri, P., Freer, M., Harper, G.S., 2012. Water footprint of livestock: comparison of six geographically defined beef production systems. Int. J. Life Cycle Assess. 17:165–175. https://doi.org/10.1007/s11367-011-0346-y.

Sauchyn, D.J., St-Jacques, J.M., Luckmanb, B.H., 2015. Long-term reliability of the Athabasca River (Alberta, Canada) as the water source for oil sands mining. PNAS U.S.A. 112 (41), 12621–12626.

Shrestha, S., Chapagain, R., Babel, M.S., 2017a. Quantifying the impact of climate change on crop yield and water footprint of rice in the Nam Oon irrigation project, Thailand. Sci. Total Environ. 599–600:689–699. https://doi.org/10.1016/j.scitotenv.2017.05.028.

Shrestha, K.S., Du, X., Wang, J., 2017b. Assessing climate change impacts on fresh water resources of the Athabasca River Basin, Canada. Sci. Total Environ. 601-602:425–440. https://doi.org/10.1016/j.scitotenv.2017.05.013.

de Souza, D.M., Petre, R., Jackson, F., Hadarits, M., Pogue, S., Carlyle, C.N., Bork, E., McAllister, T., 2017. A review of sustainability enhancements in the beef value chain: state-of-the-art and recommendations for future improvements. Animals 7:26. https://doi.org/10.3390/ani7030026.

Sun, S.K., Wu, P.T., Wang, Y.B., Zhao, X.N., 2012. Impacts of climate change on water footprint of spring wheat production: the case of an irrigation district in China. Spanish. J. Agric. Res. 10, 1176–1187.

Tan, M.L., Ibrahim, A.L., Yusop, Z., Chua, V.P., Chan, N.W., 2017. Climate change impacts under CMIP5 RCP scenarios on water resources of the Kelantan River Basin, Malaysia. Atmos. Res. 189:1–10. https://doi.org/10.1016/j.atmosres.2017.01.008.

Tuo, Y., Duan, Z., Disse, M., Chiogna, G., 2016. Evaluation of precipitation input for SWAT modeling in Alpine catchment: a case study in the Adige river basin (Italy). Sci. Total Environ. 573:66–82. https://doi.org/10.1016/j.scitotenv.2016.08.034.

Vaghefi, S.A., Mousavi, S.J., Abbaspour, K.C., Srinivasan, R., Yang, H., 2014. Analyses of the impact of climate change on water resources components, drought and wheat yield in semiarid regions: Karkheh River Basin in Iran. Hydrol. Process. 28:2018–2032. https://doi.org/10.1002/hyp.9747.

Vigiak, O., Malagó, A., Bouraoui, F., Vanmaercke, M., Poesen, J., 2015. Adapting SWAT hillslope erosion model to predict sediment concentrations and yields in large Basins. Sci. Total Environ. 538:855–875. https://doi.org/10.1016/j.scitotenv.2015.08.095.

Vrugt, J.A., Gupta, H.V., Bouten, W., Sorooshian, S., Vrugt, J.A., Gupta, H.V., Bouten, W., Sorooshian, S., 2003. A shuffled complex evolution metropolis algorithm for optimization and uncertainty assessment of hydrologic model parameters. Water Resour. Res. 39. https://doi.org/10.1029/2002WR001642.

Vu, M.T., Raghavan, S.V., Liong, S.Y., 2012. SWAT use of gridded observations for simulating runoff – a Vietnam river basin study. Hydrol. Earth Syst. Sci. 16:2801–2811. https://doi.org/10.5194/hess-16-2801-2012.

Wainwright, H.M., Jung, Y., Zhou, Q., Birkholzer, J.T., 2014. Making sense of global sensitivity analyses. Comput. Geosci. 65:84–94. https://doi.org/10.1016/j.cageo.2013.06.006.

Williams, J.R., 1995. Chapter 25: The EPIC Model In: Computer Models of Watershed Hydrology. Water Resour. Publ. Highl. Ranch. URL. http://www.scirp.org/(S(351jmbntvnsjt1aadkposzje))/reference/ReferencesPapers.aspx?ReferenceID=1153277, Accessed date: 17 May 2017.

Yang, H., Pfister, S., Bhaduri, A., 2013. Accounting for a scarce resource: virtual water and water footprint in the global water system. Curr. Opin. Environ. Sustain. 5, 599–606.